Effect of plasma on combustion characteristics of boron*

Peng Zhang(张鹏)[1,†], Wenli Zhong(钟文丽)[1], Qian Li(李倩)[1], Bo Yang(杨波)[2], Zhongguang Li(李忠光)[3], and Xiao Luan(栾骁)[4]

[1] *Department of Space Command, Space Engineering University, Beijing* 101416, *China*
[2] 63819 *Unit of People's Liberation Army, Yibin* 644000, *China*
[3] *Department of Equipment Support, Military Transportation University, Tianjin* 300161, *China*
[4] 63618 *Unit of People's Liberation Army, Korla* 841001, *China*

(Received 9 July 2017; revised manuscript received 4 August 2017; published online 29 September 2017)

As it is very difficult to release boron energy completely, kinetic mechanism of boron is not clear, which leads to the lack of theoretical guidance for studying how to accelerate boron combustion. A new semi-empirical boron combustion model is built on the King combustion model, which contains a chemical reaction path; two new methods of plasma-assisted boron combustion based on kinetic and thermal effects respectively are built on the ZDPLASKIN zero-dimensional plasma model. A plasma-supporting system is constructed based on the planar flame, discharge characteristics and the spectral characteristics of plasma and boron combustion are analyzed. The results show that discharge power does not change the sorts of excited-particles, but which can change the concentration of excited-particles. Under this experimental condition, plasma kinetic effect will become the strongest at the discharge power of 40 W; when the discharge power is less than 40 W, plasma mainly has kinetic effect, otherwise plasma has thermal effect. Numerical simulation result based on plasma kinetic effect is consistent with the experimental result at the discharge power of 40 W, and boron ignition delay time is shortened by 53.8% at the discharge power of 40 W, which indicates that plasma accelerates boron combustion has reaction kinetic paths, while the ability to accelerate boron combustion based on thermal effect is limited.

Keywords: plasma-assisted combustion, boron, ignition delay time, reaction kinetics

PACS: 05.20.Dd, 52.25.Dg, 82.33.Xj, 82.33.Vx **DOI:** 10.1088/1674-1056/26/11/110501

1. Introduction

Boron is the ideal fuel additive for solid rocket ramjet because of the high quality calorific value (58.28 kJ/g) and high volume calorific value (136.38 kJ/cm^3), which is 2.3 and 1.9 times of magnesium, 3.1 and 1.7 times of aluminum, respectively.[1] However, ignition delay time of boron is too long and combustion efficiency is too low. Boron chemical kinetic theory is not clear, which leads to the lack of theoretical guidance for studying boron combustion-supporting method.[2] Conventional combustion-supporting method, such as adding flammable metals, coating boron with strong oxidants,[3] can improve boron combustion characteristics, but there is a problem of decreasing boron chemical heat release (boron and fluoride generate BF_3, but specific heat capacity of BF_3 is very low), which will weaken boron energy advantage.[4] Plasma-assisted combustion is an effective means to realize fuel combustion with releasing heat effectively, which is one of the hotspots of aerospace development in recent years.

Plasma kinetic effect has a wide application prospect in shortening ignition delay time and improving combustion efficiency.[5] Aleksandrov *et al.* simplified the discharge mechanism. Results show that the main factor of combustion-supporting is the active particles that generate during the process of discharge, the most concentration is oxygen free radical.[6] He *et al.* established plasma kinetic model to obtain the concentration evolution of typical active particles.[7] Sun *et al.* pointed out by contrastive test that oxygen free radical is the main free radicals of plasma-insisted combustion and the starting source of fuel oxidation. More than 80% of oxygen radicals can be transported to the reaction zone to enhance multistage combustion when the temperature is beyond 900 K.[8]

Plasma can accelerate boron combustion from chemical kinetic level and avoid the problem of decreasing boron chemical heat release. However, the basic theories of plasma kinetic effect and boron combustion are not well understood.[9,10] The classical boron model cannot explain the phenomenon of plasma-assisted boron combustion. Therefore, it is of great theoretical and practical significance to study kinetic theory of plasma-assisted boron combustion and carry out theoretical innovation of this. In this paper, a boron semi-empirical model with a reaction kinetic path has been built, plasma-assisted combustion methods have been pointed out, and the rationality of model and methods has been verified by plane flame test. Which solve the problem that the existing boron semi-empirical model cannot analyze plasma-assisted boron combustion.

*Project supported by the National Natural Science Foundation of China (Grant No. 11372356).
†Corresponding author. E-mail: zhangpengtf@126.com
© 2017 Chinese Physical Society and IOP Publishing Ltd

2. Theoretical models and methods

2.1. Boron combustion model

The methods of improving boron combustion model have been studied mainly in recent years. Xia *et al.* have built a boron semi-empirical model for the influence of Stefan flow.[11] Ao *et al.* have built a boron semi-empirical model for high pressure combustion condition on King and Kuo model.[12] Which can guide theoretically the methods of boron combustion-supporting and other related research work. Kinetic model can analyze the change rules of each component from chemical reaction mechanism, but the computation is intensive and complex, and it is not suitable for the numerical study of the actual working condition of boron combustion. Therefore, it has more practical value that adding optimal mechanism to the typical boron semi-empirical model, to reflect kinetic process of boron combustion. It is the hotspot and focus in the boron combustion model development.

The boron combustion model is built on the King model in this study. The surfaces of boron particles are always covered with a layer of boron oxide (B_2O_3). Consumption of boron oxide is mainly through vaporization and reaction with water vapor. Oxygen diffusion to the interface of $B-B_2O_3$ will reacts with boron to form boron oxide. The boron ignition stage starts when the consumption of boron oxide is larger than generation, the boron combustion stage starts when boron oxide is completely consumed. The King model and parameters can refer to Ref. [13]. The main active particles of air plasma are oxygen free radicals and nitrogen oxides, and the results analysis of boron detailed mechanism show that,[14] oxygen free radicals can accelerate the oxidation reaction rate of BO. Therefore, four elementary reactions with reaction path have been added to the boron King model, which are shown as

$$\begin{aligned} &\mathrm{R0}: \ \mathrm{B}+\mathrm{B_2O_3}\rightarrow 3\mathrm{BO},\\ &\mathrm{R1}: \ \mathrm{O_2}+\mathrm{M}\rightarrow \mathrm{O}+\mathrm{O}+\mathrm{M},\\ &\mathrm{R2}: \ \mathrm{BO}+\mathrm{O}\rightarrow \mathrm{BO_2},\\ &\mathrm{R3}: \ \mathrm{BO_2}+\mathrm{BO}\rightarrow \mathrm{B_2O_3}. \end{aligned} \tag{1}$$

2.1.1. Assumptions

The following assumptions are needed to calculate elementary reaction rate.

1) Boron particles are uniform spheres; the surfaces of pure boron are covered with a layer of boron oxide (B_2O_3).

2) O, BO, and BO_2 are already evenly distributed in the boron oxide layer.

3) BO is kinetic controlled by reactions of R1, R2, and R3.

4) The third body M is any other components except O_2.

2.1.2. Reaction rate of elementary reaction

(I) Equilibrium reaction of $B_{(s)}$ with $B_2O_{3(l)}$. The elementary reaction (R0: $B_{(s)}+B_2O_{3(l)}\rightarrow 3BO_{(l)}$) is an equilibrium reaction, which cannot be the rate-limiting step, there is no rate-limiting problem, the reaction rate is given as that in Ref. [15]. The n_{BO} is the amount of substance of $BO_{(l)}$ as

$$\begin{aligned} n_{\mathrm{BO}} &= n_{\mathrm{Z}}\chi_{\mathrm{BO}} = 2.32\times 10^{-2}\left(\frac{\left(4\pi r_{\mathrm{B}}^3/3\right)\rho_{\mathrm{B(s)}}}{M}{}_{\mathrm{B(s)}}\right.\\ &\quad \left.+\frac{4\pi r_{\mathrm{B}}^2 X\rho_{\mathrm{B_2O_3}}}{M_{\mathrm{B_2O_3}}}\right)\\ &\quad \times\left(1-\exp\left(\frac{3500}{T_{\mathrm{P}}}-\frac{3500}{T_{\mathrm{cut}}}\right)\right), \end{aligned} \tag{2}$$

where χ_{BO} is the equilibrium mole fraction of $BO_{(l)}$ at the $B_{(s)}/B_2O_{3(l)}$ interface, n_Z is the amount of substance of $B_2O_{3(l)}$. The expressions of χ_{BO} and n_Z are

$$\chi_{\mathrm{BO}} = 2.32\times 10^{-2}\left(1-\exp\left(3500/T_{\mathrm{P}}-3500/T_{\mathrm{cut}}\right)\right), \tag{3}$$

$$\begin{aligned} n_{\mathrm{Z}} &= m_{\mathrm{B(s)}}/M_{\mathrm{B(s)}}+m_{\mathrm{B_2O_3}}/M_{\mathrm{B_2O_3}}\\ &= \left(4\pi r_{\mathrm{B}}^3/3\right)\rho_{\mathrm{B(s)}}/M_{\mathrm{B(s)}}+4\pi r_{\mathrm{B}}^2 X\rho_{\mathrm{B_2O_3}}/M_{\mathrm{B_2O_3}}, \end{aligned} \tag{4}$$

where T_{cut} is the temperature above which the hoxide layer removal occurs by chemical reactions, and $T_{cut}=1550$ K at the condition of this study.

The elementary reactions (R1–R3) are the rate-limiting reactions, the reaction rates can be expressed in the Arrhenius form, which are givenin Ref. [16].

(II) Elementary reaction (R1): $O_2+M=O+O+M-Q_{R1}$,

$$k_1 = 1.81\times 10^{18}T_{\infty}^{-1}\exp\left(-118100/(1.987T_{\infty})\right), \tag{5}$$

where k_1 is the reaction rate constant for the reaction (R1), $cm^3/(mole\cdot s)$, and

$$\begin{aligned} &R_1 = 4\pi r_{\mathrm{B}}^2 X k_1\left[O_2\right]\left[M\right],\ \mathrm{mole/s},\\ &Q_{\mathrm{R1}} = 119.10\times 10^3,\ \mathrm{cal/mole}, \end{aligned} \tag{6}$$

where R_1 is the molar reaction rate by the reaction (R1), mole/s; Q_{R1} is the heat absorbed by the reaction (R1), cal/mole.

(III) Elementary reaction (R2): $BO+O+M=BO_2+M+Q_{R2}$,

$$k_2 = 1.1\times 10^{15}\exp\left(1990/(1.987T_{\mathrm{P}})\right), \tag{7}$$

where k_2 is reaction rate constant for the reaction (R2), $cm^6/(mole^2\cdot s)$, and

$$\begin{aligned} &R_2 = 4\pi r_{\mathrm{B}}^2 X\alpha_2 k_2\left[\mathrm{BO}\right]\left[\mathrm{O}\right]\left[\mathrm{M}\right],\ \mathrm{mole/s},\\ &Q_{\mathrm{R2}} = 127.55\times 10^3,\ \mathrm{cal/mole}, \end{aligned} \tag{8}$$

where R_2 is the molar reaction rate by the reaction (R2), mole/s; Q_{R2} is the heat released by the reaction (R2), cal/mole; α_2 is the reaction probability of the reaction (R2), $\alpha_2=0.035$; O should be more than consumption as

$$\frac{\mathrm{d}n_{\mathrm{BO}}}{\mathrm{d}t} = n_{\mathrm{BO}}-(R_2+R_3)\geq 0. \tag{9}$$

(IV) Elementary reaction (R3): $BO + BO_2 + M = B_2O_3 + M + Q_{R3}$,

$$k_3 = 7.24 \times 10^{13} \exp\left(1990/(1.987 T_P)\right), \tag{10}$$

where k_3 is the reaction rate constant for the reaction (R3) $cm^6/(mole^2 \cdot s)$, and

$$R_3 = 4\pi r_B^2 X \alpha_3 k_3 [BO][BO_2][M],$$
$$Q_{R3} = 131.80 \times 10^3, \text{ cal/mole}, \tag{11}$$

where R_3 is the molar reaction rate of the reaction (R3), mole/s; Q_{R3} is the heat released of the reaction (R3), cal/mole; α_3 is the reaction probability of reaction (R3), $\alpha_3 = 0.35$; BO_2 should be more than consumption as

$$\frac{dn_{BO_2}}{dt} = R_2 - R_3 \geq 0. \tag{12}$$

2.1.3. Modified governing equation

Boron mass balance equation is

$$\frac{dr_B}{dt} = -\frac{[\lambda(R_2 + R_3) + (1-\lambda)R_B]M_B}{4\pi r_{B^2}\rho_B}. \tag{13}$$

Boron oxide mass balance equation is

$$\frac{dX}{dt} = \frac{[(1-\lambda)(R_B/2 - R_E - R_H) - \lambda(R_2 + R_3)]M_{B_2O_3}}{4\pi r_B^2 \rho_{B_2O_3}}, \tag{14}$$

and Q_1 and Q_2 are the heat released as

$$\begin{aligned} Q_1 &= [(1-\theta)(R_{BQ_{B1}-R_EQ_E-R_HQ_H}) + \theta(R_2Q_{R2} + R_3Q_{R3})] \\ &\quad + 4\pi r_P^2 \left[h(T - T_P) + \sigma\varepsilon\alpha_R\left(T_{RAD}^4 - T_P^4\right)\right], \\ Q_2 &= [(1-\theta)(R_{BQ_{B2}-R_EQ_E-R_HQ_H}) + \theta(R_2Q_{R2} + R_3Q_{R3})] \\ &\quad + 4\pi r_P^2 \left[h(T - T_P) + \sigma\varepsilon\alpha_R\left(T_{RAD}^4 - T_P^4\right)\right], \end{aligned} \tag{15}$$

where θ is the consumption via by the reactions R2 and R3 account for the total boron oxide consumption, $\theta = \chi_{BO}/3$; $[x]$ is the molar concentration of component x, mole/cm^3; r_B is the boron particle radius, X is the thickness of the boron oxide layer, cm; T_P is the temperature of boron, T is the flame temperature of the burner, T_{RAD} is the radiation temperature of surroundings, K; M_B is boron atomic weight, M_B=10.82 g/mol; ρ_B is boron density, $\rho_B = 2.33$ g/cm^3; $M_{B_2O_3}$ is boric oxide molecular weight, $M_{B_2O_3} = 69.64$; $\rho_{B_2O_3}$ is boric oxide density, $\rho_{B_2O_3} = 1.85$ g/cm^3; σ is Stefan–Boltzmann constant, $\sigma = 1.354 \times 10^{-12}$ cal/($cm^2 \cdot s \cdot K^4$); $c_{p_{B_2O_3}}$ is liquid boron oxide heat capacity, $c_{p_{B_2O_3}} = 0.438$ cal/(g·K); $c_{p_{B(s)}}$ is solid boron heat capacity, $c_{p_{B(s)}} = 0.507 + 7.0 \times 10^{-5} T_p$ cal/(g·K); $c_{p_{B(l)}}$ is liquid boron heat capacity, $c_{p_{B(l)}} = 0.675$ cal/(g·K).

2.2. Plasma-assisted methods

2.2.1. Plasma kinetic analysis method

The plasma discharge process is an activation process of neutral particles and electron energy transfer. Electron energy will be converted to the bond energy of free radicals, after a series of reactions such as collision, excitation, dissociation, ionization, charge exchange, quenching of excited state particles, and recombination of electrons–ions.[17] The free radicals generated in the discharge phase are simulated based on the ZDPLASKIN zero-dimensional plasma kinetic model. The control equations are

$$\frac{d[N_i]}{dt} = \sum_{j=1}^{j_{max}} Q_{ij}(t), \tag{16}$$

$$aA + bB[+\delta\varepsilon] \rightarrow a'A + cC[+\delta\varepsilon], \tag{17}$$

$$R_j = k_j [N_A]^a [N_B]^b, \tag{18}$$

$$Q_A = (a' - a)R; \quad Q_B = -bR; \quad Q_C = cR. \tag{19}$$

The energy transfer process of temperature change is described by the adiabatic isometric approximation equation, ignoring the Joule heat generated by the ion motion

$$\frac{[N_{gas}]}{\gamma - 1}\frac{dT_{gas}}{dt} = \sum_{j=1}^{j_{max}} \pm\delta\varepsilon_j R_j + P_{elast}[N_e], \tag{20}$$

where $[N_i]$ is the density of component N_i, Q_{ij} is the rate of density change going from reactant i to product j, j_{max} is the maximum of product j; A, B, C are reaction components; a, a', b, c are stoichiometric number, $[+\delta\varepsilon]$ is chemical reaction calorific value; R_j is the reaction rate of component j, k_j is the reaction rate constant of component j; $[N_A]$ is the density of component A, $[N_B]$ is the density of component B; Q_A, Q_B, Q_C are the density change rates of components A, B, C; R is the reaction rate; $[N_{gas}]$, γ, T_{gas}, P_{elast}, $[N_e]$ are gas density, adiabatic exponent, gas temperature, electron impact energy, electron density; $\delta\varepsilon_j$ is the chemical reaction calorific value of reaction j.

2.2.2. Plasma thermal analysis method

The effect of plasma on the gas temperature is mainly based on the energy of electron impact loss and reaction heat absorption and release. Considering only the thermal effect of plasma, the effect of reaction heat absorption and release is removed, and the whole discharge energy is used to change the ambient temperature and radiation temperature of the gas around boron particles, and the modified energy transfer equation is

$$\frac{dT_{P-RAD}}{dt} = \frac{\gamma - 1}{[N_{gas}]}P_{power}, \tag{21}$$

where T_{P-RAD} is the temperature increased by discharge, K; P_{power} is the discharge power of plasma, eV.

3. Experimental analysis methods

3.1. Experimental system

The experimental system consists of a particle combustion system, a plasma system, and a measurement and diagnosis system. The particle combustion system includes a multi-diffusion planar flame burner (a post-flame instantaneous heating particle produced by methane combustion), a boron particle feeding device and a gas supply device; the plasma system includes a needle-like plasma exciter and a high-frequency high-voltage power supply; the measurement and diagnosis system includes an image analysis system, a spectral diagnosis system, and a discharge characteristic analysis system. The multi-diffusion planar flame burner is divided into upper and lower layers, and the lower layer is methane, which is rectified into the capillary metal tube (inner diameter 0.8 mm, outer diameter 1 mm); the upper layer is a certain proportion of mixed nitrogen and oxygen, which flows out from the honeycomb holes around the capillary tube, and forms a flat flame with methane; boron particles are dissolved in a certain proportion to ethanol, which are fully dispersed after vibrating and will enter the dryer in the form of aerosol after atomizing, and finally boron particles are loaded by nitrogen into the central tube of the honeycomb and will be heated by methane combustion to form boron flame, the whole experimental system is shown in Fig. 1.

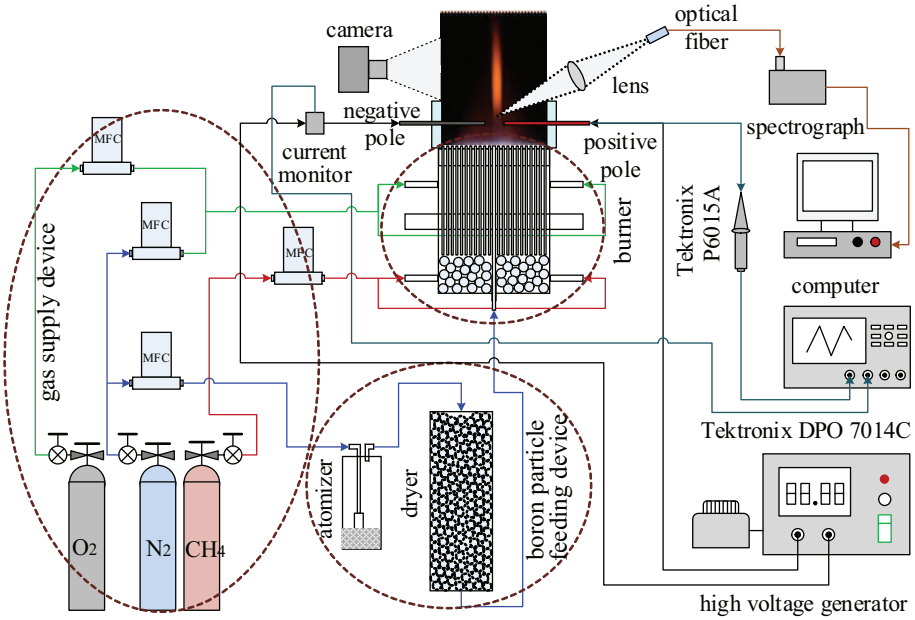


Fig. 1. (color online) Experimental system diagram.

The high frequency and high voltage power supply is produced by Nanjing Suman Company, model CTP-2000K, output voltage 0–30 kV, frequency 10 kHz; high voltage probe is produced by Tektronix company, model P6015A, rise time 14 ns, bandwidth 75 MHz, peak voltage 40 kV; the current coil is produced by Pearson Company, model P6595, peak current 10 A, rise time 20 ns; oscilloscope is produced by Tektronix Company, bandwidth 500 MHz, sampling frequency 5.0 GS/s; HR4000CG-UV-NIR broadband spectrometer is used in this study, bandwidth 200–1100 nm, the composite grating of 5 μm incident slit, the filter of eliminating high-order diffraction, the optical resolution of 0.7 nm FWHM.

3.2. Boron flame image analysis method

3.2.1. Image analysis principle

Planck gives the quantitative relationship between the blackbody radiation and the object surface temperature. It is pointed out that, when the particle temperature is lower than 3000 K and the radiation wavelength range is 400–800 nm, the radiation energy $I(\lambda, T_{\mathrm{P}})$, the spectral characteristic wavelength λ, and the particle temperature T_{P} can be expressed as[18]

$$I(\lambda, T_{\mathrm{P}}) = \varepsilon(\lambda, T_{\mathrm{P}}) \frac{C_1 \lambda^{-5}}{\mathrm{e}^{(C_2/\lambda T_{\mathrm{P}})} - 1}, \tag{22}$$

where C_1 and C_2 are the first and second radiation constants; $\varepsilon(\lambda, T_{\mathrm{P}})$ is the particle emissivity, which is used to correct the difference between particle combustion radiation and blackbody radiation.

The three band signals (red, green, and blue) which are extracted from the SLR camera can be reduced to the corresponding peak wavelengths, and the band radiation will be considered approximately as the wavelength radiation. Particle combustion radiation is dominated by the continuous thermal radiation and the fluorescent radiation of the active particles, and the flame image stores all the radiation signals,[19]

which can be expressed as

$$S(z,T_{\rm P}) = \tau_{\rm expose} N_{\rm P} \int 4\pi r_r^2 I(\lambda,T_{\rm P})\,\eta(\lambda)\,{\rm d}\lambda, \qquad (23)$$

where z, $N_{\rm P}$, and $r_{\rm r}$ are the spatial dimension of each pixel, the corresponding particle concentration of each pixel, and the corresponding physical radius of each pixel; $\tau_{\rm expose}$ and $\eta(\lambda)$ are the exposure time and the energy conversion rate, respectively.

The thermal radiation is mainly concentrated in the red band at the temperature in the range of 1000–3000 K, which can represent the particle temperature;[20] Yu *et al.* pointed out that the green band is the main color of the BO_2 emission spectrum, the single value function of green and red signal ratio, which can indicate the sensitivity of the BO_2 generation rate to temperature, in other word, the degree of boron burning as[21]

$$\frac{S_G(z,T_{\rm P})}{S_R(z,T_{\rm P})} = \frac{\int_G I(\lambda,T_{\rm P})\,\eta_G(\lambda)\,{\rm d}\lambda}{\int_R I(\lambda,T_{\rm P})\,\eta_R(\lambda)\,{\rm d}\lambda} = f(z,T_{\rm P}), \qquad (24)$$

where subscripts G and R are only the spectral radiation information of green and red, respectively.

It should be noted that only the relative strength of radiation intensity and flame two-dimensional space size are needed to consider in this study, so calibrating the absolute temperature is not necessary. The experimental results are mainly related to the three-band radiation information represented by the CMOS spectral response curve, and have no concern with the camera lens, imaging systems, operating modes, and color reproduction capability.

3.2.2. Boron combustion stage division method

The combustion process of boron particles is generally divided into three stages: ignition delay, ignition, and combustion. The three kinds of information of red, green, and blue and the spatial size of each pixel can be extracted from the boron flame image by MATLAB software. The red radiation (red band) and BO_2 emission spectrum (green band) of boron particles along the flame propagation direction are analyzed, boron combustion stage division method is shown in Fig. 2.

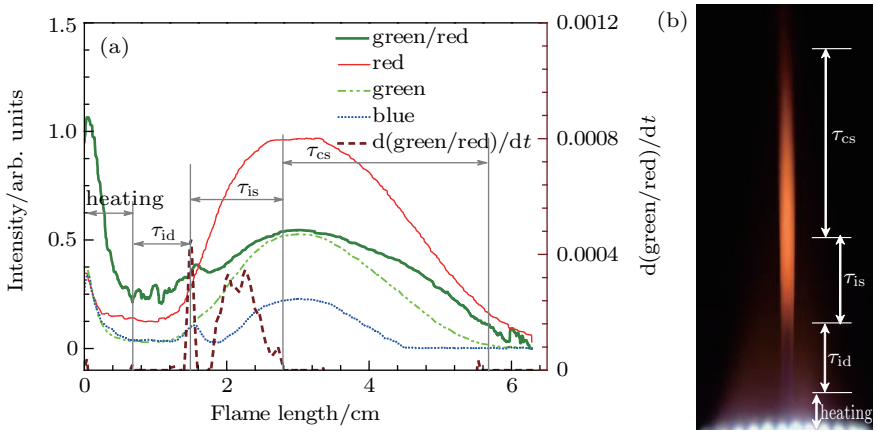


Fig. 2. (color online) Three-phase diagram division method of boron particle combustion. (a) The color information of boron flame image and (b) flame image of boron.

A typical boron combustion flame image obtained in this experiment is shown in Fig. 2(b). Temperature of boron particles reaches the ignition temperature when particles flow the distance of 8 mm. By then, boron particles will be in ignition delay, ignition, and combustion stages one after another. The information curves of red, green, and blue with the flame height are extracted from the boron flame image, where "green/red" represents the degree of particle combustion, d(green/red)/dt represents the slope of the degree of particle combustion change curve.

Ignition delay time $\tau_{\rm id}$ is defined as the time required for boron particles reaching the ignition temperature to the peak slope of the combustion degree; ignition time $\tau_{\rm is}$ is defined as the time required for the peak slope of the combustion degree to the peak point of the combustion degree; and combustion time $\tau_{\rm cs}$ is defined as the time required for the peak point of the combustion degree to 20% of the peak point of the combustion degree.

It can be seen from Fig. 2(a) that there is a strong radiation at the flame distance of 0 mm, the reason is that the plane flame is a methane combustion zone and generates a large number of active particles (such as C, C_2, C_3, etc.), and the emission spectrum within the wavelength range of 500–580 nm is strong; and it is mainly the spectral information of boron combustion when the flame height is more than 8 mm, that is why it is necessary to judge the boron combustion stage with the flame height of more than 8 mm. The resolution of flame image is 6016×4016 in this study, and the high resolution of the two-dimensional space ensures the time accuracy of three combustion stages.

3.2.3. Particle flow rate characterization method

Combustion time t is obtained by dividing the boron flame length l by the boron flow rate ($t = l/v_p$). Yeh *et al.* measured boron particle flow trajectories, and indicated that the particle velocity at the moment of injection is extremely high and then reduces until reaching the ignition delay time, ignition, and combustion zones, where the particle rate will be basically stable in the constant, so the average can be taken as the particle rate.[22] The size of boron particle is very small (only a few micrometer) in this study, which is better with gas flow. It is assumed that the boron particle rate is the same as the gas flow rate, so the boron particle rate will be estimated according to the gas flow velocity, and the formula is

$$v_p = v_{gas} = \frac{Q_0}{6 \times 10^4 \pi r_{eff}^2} \times \frac{T}{T_{g,0}}, \tag{25}$$

where v_p is the particle rate, m/s; v_{gas} is the gas rate, m/s; Q_0 is the gas flow through the central tube, SLM (standard liter per minute); r_{eff} is the effective radius of the particles jet, mm; T is the ambient temperature, K; $T_{g,0}$ is the standard ambient temperature, 273.15 K. The consistency between the numerical values and experimental results obtained by the laser phase doppler analyzer ensures the rationality of this formula.

4. Results and discussion

4.1. Experimental process

Firstly, boron particles are dispersed in a certain proportion to ethanol solution (mass ratio 1: 80); secondly, boron particle suspensions need two hours of ultrasonic oscillations, so that particles are more fully dispersed; thirdly, boron particles and ethanol need to be atomized by aerosol and blown in the $CaCl_2$ diffusion dryer in the form of gasoloid, so that ethanol and other liquids will be removed; and finally, boron particles blow in the high temperature zone of methane combustion from the bottom of honeycomb center of the stainless steel tube (diameter 2 mm).

Plasma in this study is needle-like arc discharge plasma (two tungsten electrodes are the high voltage pole and ground pole, tungsten pole diameter is 1.6 mm), the electrode spacing is 4 mm, and the distance from the burner surface is 8 mm. A high-voltage probe and a current coil are used to measure the discharge voltage and current respectively, and the discharge power can obtained by integral; a spectrometer is used to measure boron flame spectrum; the color SLR camera is used to photograph the flame of boron particles.

4.2. Experimental results

A typical experimental condition in this study is as follows: CH_4 flow 0.92 SLM, O_2 flow 7.36 SLM, N_2 flow 6.92 SLM. The component of flame zone is N_2: O_2: CO_2: H_2O = 0.455:0.362:0.061:0.122, and the temperature is 1575 K; the nitrogen flow rate in the honeycomb center stainless steel tube is $Q_0 = 0.50$ SLM and boron particle flow rate is 15.3 m/s.

Discharge power is a typical plasma characteristic that affects the combustion characteristics of boron. Discharge voltage and current signals at both ends of the plasma exciter are measured, discharge power is calculated by voltage and current integral, and the frequency of the high-frequency high-voltage power supply is 11.0 kHz in this study. The Savitzky–Golay filtered voltage and current signals are shown in Fig. 3.

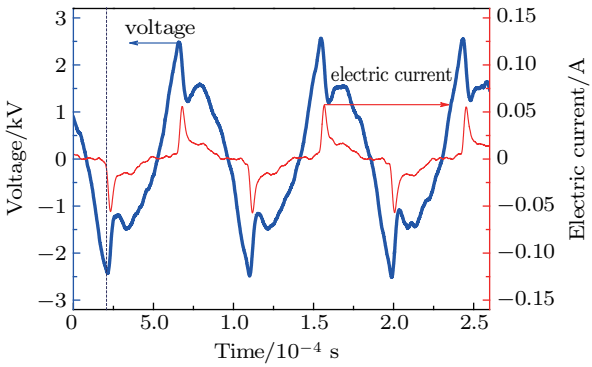


Fig. 3. (color online) Waveforms of the discharge voltage and current.

It can be seen from Fig. 3 that the current increases as the voltage increases (the current is approximately zero before the voltage reaches the breakdown voltage, and the discharge energy is approximately zero at that moment). It will generate arc plasma when the voltage reaches the breakdown voltage, the current instantaneously increases to the peak, and then the voltage decreases with the increase of electric conductance between arcs, and then the current begins to decrease. Arcs will extinguish and the arc conductance instantaneously decreases when the current decreases to approximately zero, and then voltage increases to the breakdown voltage from reverse, the discharge process goes on.

Figure 4 is the boron flame photos under a series of typical discharge powers with the use of Nikon D610, aperture F4, ISO 800, white balance sun and shutter 1/5 s. Arc breakdown position is fixed when the discharge power is greater than 10 W. The arc near the electrode side is brighter and which temperature is higher; the arc column end which acts on the boron flame is relatively dark and the temperature is much lower. The concentration of active particles increases, boron flame is brighter and ignition delay time is obviously shortened when discharge power increases.

Plasma kinetic effect refers to the collision of high energy electrons with neutral particles, excitation, dissociation and even ionization, to generate large amounts of active particles (such as free radicals, charged ions, excited molecules and atoms), to improve the elementary reaction rate. Emission spectrum is one of the primary means of measuring and

diagnosing active particles, which can measure relevant information without affecting the working state of the test source. The principle is that molecules, atoms, and ions of the high energy states transition to the low energy states, and the excess energy will be released. Fiber optic probe aims at the needle electrode arc column position through lens in this study, plasma spectrum characteristics under typical discharge powers are shown in Fig. 5, and the integration time is 2 s.

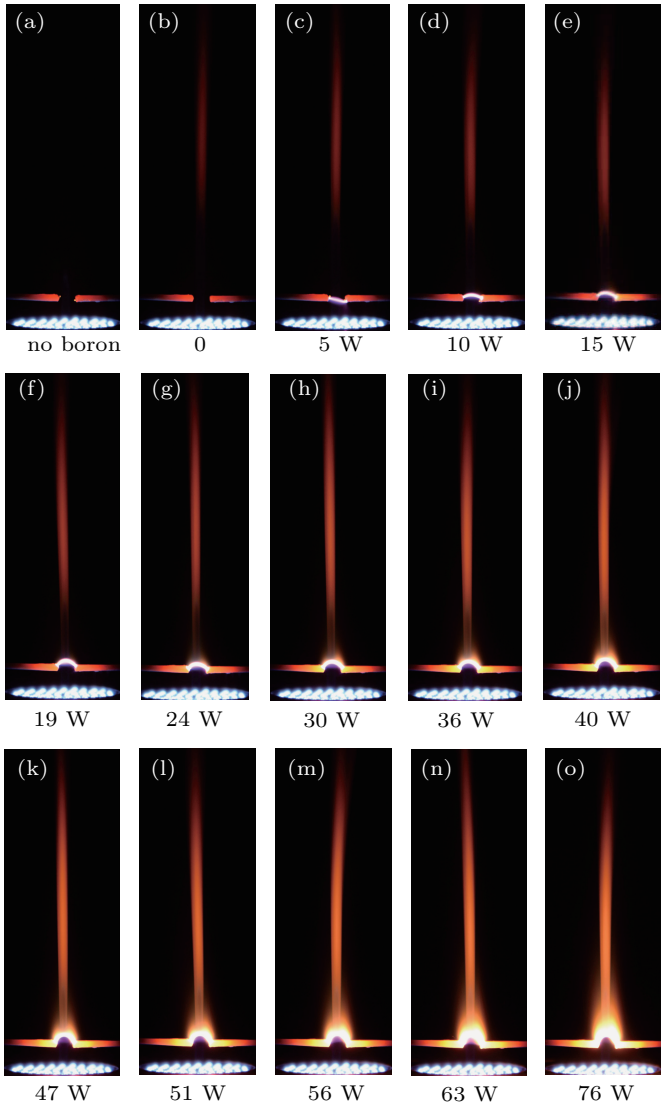


Fig. 4. (color online) Boron combustion flame images under different discharge power levels. (a) No boron, (b) 0, (c) 5 W, (d) 10 W, (e) 15 W, (f) 19 W, (g) 24 w, (h) 30 W, (i) 36 W, (j) 40 W, (k) 47 W, (l) 51 W, (m) 56 W, (n) 63 W, (o) 76 W.

As can be seen from Fig. 5, the types of active particles does not change but the concentrations change with the increase of discharge power, the peak wavelength is 367.1 nm of $O_2\left(B^3\Sigma_u^- - X^3\Sigma_g^-\right)$. Thermal radiation spectrums mainly exist in the wavelength scope of 450–1000 nm, which reflects plasma thermal effect; the fluorescent radiation of active particles mainly exist in the wavelength scope of less than 450 nm, which reflects plasma kinetic effect. Thermal radiation spectrum intensities increase progressively and plasma thermal effect is stronger with the increase of discharge power; plasma kinetic effect increases at first and then decreases, which reaches the peak at the discharge power of 40 W. Plasma mainly has the kinetic effect and the concentration of active particles is larger when the discharge power is less than 40 W; plasma mainly has the thermal effect and the concentration of active particles is far less when the discharge power is more than 40 W. The emission spectrum intensity of 367.1 nm is 24260 at the discharge power of 40 W, while the intensity will be reduced to 19710 with the discharge power of 51 W, in other word, the concentrations of active particles decrease by 18.7% when the power increases by 25% under this concentration.

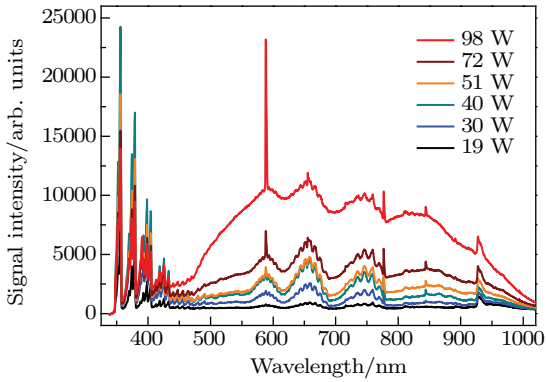


Fig. 5. (color online) Plasma emission spectrum under different discharge power levels.

The main emission spectra are: the spectrum 367.1 nm and 373.4 nm of oxygen molecules $O_2(B^3\Sigma_u^- - X^3\Sigma_g^-)$ and $O_2(A^3\Sigma_u^+ - X^3\Sigma_g^-)$; the N_2 positive bands are generated by transition (313.62 nm, 315.81 nm, 337.13 nm, 353.69 nm, 357.73 nm, 370.98 nm, 375.06 nm, 380.06 nm, 394.18 nm, 399.22 nm, 405.77 nm); and the emission spectra of active particles such as CH, C, C_2, C_3, C_5, C^+ are mainly focused on 580 nm, 650 nm, and 750 nm, which will improve the particle concentration, and enhance the emission spectrum intensity.

The main controlling factor of boron combustion is the oxidation rate of BO, and BO is mainly oxidized to BO_2. The spectral characteristics of BO_2 are measured and the combustion characteristics of boron particles under typical discharge power are analyzed in this study. Measurement results are shown in Fig. 6, and the emission spectra of BO_2 wavelengths (452.7 nm, 471.4 nm, 493.2 nm, 517.7 nm, 547.0 nm, 578.5 nm, 602.3 nm, 619.7 nm, 638.0 nm) are obtained by focusing the optical fiber probe of spectrometer at 20 mm above the exit of boron particles, integral time 2 s, and the wavelength of 547.0 nm is the strongest. In addition, the spectrum characteristic of Na (589.7 nm) will be produced in this experimental system at high temperature, since the experimental apparatus contains sodium element.

It can be seen from Fig. 6 that the peak of BO_2 spectrums is constant, but the spectral intensity is enhanced with the in-

crease of the discharge power, which indicates that the oxidation of BO, the concentration of BO_2, and the boron combustion reaction rate can be increased with the increase of discharge power. When the discharge power is 40 W (plasma mainly has the kinetic effect), the spectral intensity of BO_2 wavelengths (602.3 nm, 619.7 nm, 638.0 nm) is higher than that in the discharge power of 47 W (plasma mainly has the thermal effect), which indicates that plasma has a reaction path for assisting boron combustion.

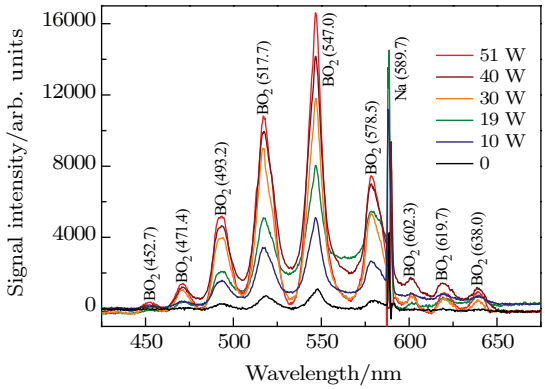


Fig. 6. (color online) Boron emission spectrum under different discharge power levels.

4.3. Results analysis

The rationality of theoretical model is verified by contrasting the classical king model in the classical literature. The initial conditions are: particle diameter $r_P = 10$ μm, oxide layer B_2O_3 thickness $X = 0.1$ μm, particle temperature $T_P = 1800$ K, ambient temperature $T_{RAD} = 2100$ K, $T_\infty = 2100$ K, oxygen mole fraction 0.2, ambient pressure $P_0 = 1$ atm, and numerical results are shown in Fig. 7. The oxide layer continues to decrease until it disappears completely and the oxide releases more heat. Ignition delay time is defined as the time that the thickness of oxide layer is reduced to 10%. The simulated temperature and oxide thickness curves in this study are the same as those of the King model. The sum of ignition delay time and ignition time is 4.6 ms, and the time is reduced by 24% when adding 0.1% O radical.

Particle velocity is 15.3 m/s, time is 0.523 ms, and temperature is 1311 K when boron particles move to the plasma region (8 mm from the burner center hole) in this experimental condition, ignoring the influence of transport (convection and diffusion) factors. Pure boron diameter 2×10^{-4} mm, oxide layer thickness 1×10^{-6} mm, experimental and numerical results are shown in Fig. 8. The diameter of boron particles are mainly in 2.0 μm and boron purity is 99.99%. The thickness of oxide layer in the literature is mostly an estimated value (0.01–0.1 μm); but the thickness of oxide layer directly affects ignition delay time of boron particles, so the selection of estimated values is very important. The thickness of oxide layer covering on the surface of boron particles is obtained by transmission electron microscopy (TEM) in this study, which is 0.02 μm.

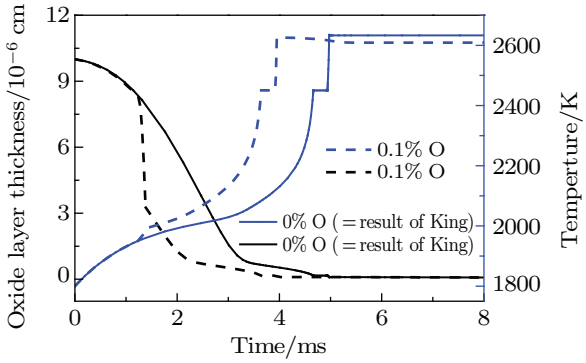


Fig. 7. (color online) Computational results of this study.

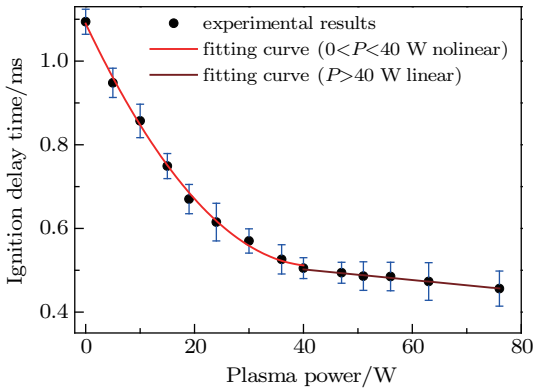


Fig. 8. (color online) Experimental results of ignition delay time.

As can be seen from Fig. 8, the ignition delay time decreases with the discharge power increases. Plasma mainly reflects the kinetic effect when the discharge power is less than 40 W. Plasma produces active particles (mainly O radicals), which can bypass the chain initiation of boron burning, break the equilibrium of chain termination, strengthen directly the chain ranch and propagation, and finally increase the reaction rate. Plasma mainly reflects the thermal effect when the discharge power is greater than 40 W, which will shorten the relative reduced amplitude of boron ignition delay time. The curve fitting is obtained by the software of ORIGIN, and polynomial fitting model functions are used, the fitting equation is

$$\tau_{id} = \begin{cases} 3.252 \times 10^{-4} P_{power}^2 - 0.028 P_{power} + 1.086, & (0 \le P_{power} \le 40\ \mathrm{W}), \\ -0.002 P_{power} + 0.599, & (40 < P_{power} \le 76\ \mathrm{W}). \end{cases} \tag{26}$$

Figure 9 shows the numerical results under the same experimental conditions. The magnitude of plasma shortens ignition delay time is very small, from 1.10 ms to 0.83 ms, when plasma energy is fully converted to heat (thermal effect). The magnitude of plasma shortens ignition delay time is large, from 1.10 ms to 0.41 ms, when plasma energy is fully used for all electrons to produce active particles (kinetic effect). Ignition delay time is shortened by 53.8% when the discharge power is 40 W, which gets better consistency with the experimental result. It is shown that there is a reaction path of plasma-assisted boron combustion, and the rationality of this improved boron semi-empirical model is verified.

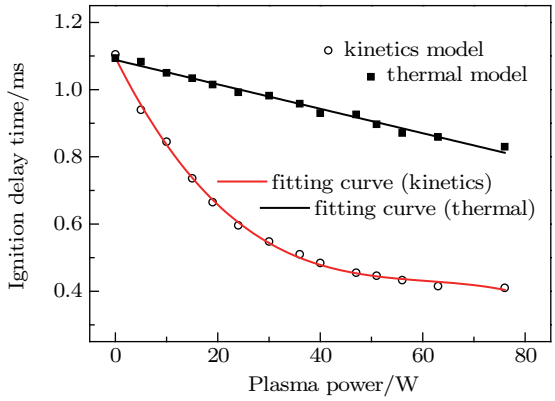


Fig. 9. (color online) Computational results of ignition delay time.

When plasma mainly reflects the thermal effect, the fitting equation of ignition delay time with the discharge power is

$$\tau_{\mathrm{id}} = -0.004\,P_{\mathrm{power}} + 1.088, \quad \left(0 \le P_{\mathrm{power}} \le 76\ \mathrm{W}\right). \quad (27)$$

When plasma mainly reflects the kinetic effect, the fitting equation of ignition delay time with the discharge power is

$$\tau_{\mathrm{id}} = -2.64 \times 10^{-6} P_{\mathrm{power}}^{3} + 4.82 \times 10^{-4} P_{\mathrm{power}}^{2} - 0.03 P_{\mathrm{power}} + 1.095, \quad \left(0 \le P_{\mathrm{power}} \le 76\ \mathrm{W}\right). \quad (28)$$

5. Conclusion and perspectives

Ignition delay time of plasma-assisted boron combustion is analyzed by plane flame test, spectral diagnosis technique and kinetic simulation. Reaction kinetic mechanism of plasma-assisted boron combustion is revealed, reaction paths of plasma-assisted combustion are pointed out, and the problem of existing semi-empirical boron model cannot be analyzed from the reaction kinetic mechanism is solved. The main conclusions are as follows.

The radiation signal intensity ratio (green/red) is strengthened and then weakened with the increase of boron flame height, and the three stages of boron combustion can be characterized; the green signal shows the emission spectrum of active particles BO_2, the red signal indicates the thermal radiation of boron combustion.

Plasma mainly has the kinetic effect when the discharge power is less than 40 W, the typical spectral intensity increases with the increase of the discharge power, the peak is in the 40 W; plasma mainly has the thermal effects when the discharge power is larger than 40 W, the thermal radiation is enhanced and the intensity of active particles decreases under this experimental condition. Discharge intensity does not change the excitation particles of plasma and BO_2, but changes the particle concentration. The spectral intensity of BO_2 (wavelength 602.3 nm, 619.7 nm, 638.0 nm, etc.) in the discharge power of 40 W is higher than that in the discharge power of more than 40 W, which indicates that plasma has a reaction path that assisting boron combustion.

The numerical result based on plasma kinetic effect gets better consistency with the experimental result at the discharge power of 40 W. Ignition delay time of boron is shortened by 53.8%, which indicates that plasma-assisted boron combustion has a reaction kinetic path, and the combustion-supporting of kinetic effect is stronger than thermal effect obviously.

References

[1] Beckstead M W, Puduppakkam K, Thakre P and Yang V 2007 *Prog. Energ. Combust.* **33** 497
[2] Fry R S 2004 *J. Propul. Power* **20** 27
[3] Mi X M, Goroshin S, Higgins J A, Stowe R and Ringuette S 2013 *Combust. Flame* **160** 2608
[4] Fomin M V, Zvegintsev I V, Mazhul I I and Shumskii V V 2010 *J. Appl. Mech. Tech. Ph.* **51** 792
[5] Ju Y G and Sun W T 2015 *Prog. Energ. Combust.* **48** 21
[6] Aleksandrov N L, Kindysheva S V and Kochetov I V 2014 *Plasma Sources Sci. Techol.* **23** 015017
[7] He L M, Liu X J, Ding W, Shen Y, Wang F and Song Z X 2012 *High Volt. Engin.* **38** 1126
[8] Sun W, Sang H W and Ju Y 2014 *Combust. Flame* **161** 2054
[9] Askarova S A, Karpenko I E, Messerle E V and Ustimenko B A. 2006 *High Energ. Chem.* **40** 141
[10] Alimi R and Berdichevsky V 2007 *Propellants. Explos. Pyrotech.* **32** 514
[11] Fang C B, Xia Z X, Xiao Y L, Hu J X and Liu D P. 2013 *Acta Phys. Sin.* **62** 164702
[12] Ao W, Yang W J, Wang Y, Zhou J H, Liu J Z and Cen K F 2014 *J. Propul. Power* **30** 760
[13] Zhang P, Hong Y J, Ding X Y, Shen S Y and Feng X P 2015 *Acta Phys. Sin.* **64** 205203
[14] Zhang P, Hong Y J, Ding X Y, Shen S Y and Yang B2015 *J. Propul. Technol.* **36** 1582
[15] Yeh C L and Kuo K K 1996 *Energy Combust. Sci.* **22** 511
[16] Pastenack L 1992 *Combust. Flame* **90** 259
[17] Yu J L, He L M, Ding W, Wang Y Q and Du C 2013 *Chin. Phys. B* **22** 055201
[18] Fu T R, Yang Z J and Cheng X F 2009 *Chin. Soc. Elec. Eng.* **29** 81
[19] Kong C D, Yu D, Yao Q, Zhuo J K and Li S Q 2015 *Opt. Precision Eng.* **23** 2288
[20] Trunov M A, Schoenitz M, Zhu X M and Dreizin E L 2005 *Combust. Flame* **140** 310
[21] Kong C D, Yao Q, Yu D and Li S Q 2015 *P. Combust. Inst.* **35** 2479
[22] Yeh C L and Kuo K K 1996 *Prog. Energ. Combust.* **22** 511